Eur. J. Phys. **20** (1999) 1–14. Printed in the UK PII: S0143-0807(99)95676-3

Black plastic sandwiches demonstrating biaxial optical anisotropy

Michael Berry†, Rajendra Bhandari‡ and Susanne Klein†

† H H Wills Physics Laboratory, Univeristy of Bristol, Tyndall Avenue, Bristol BS8 1TL, UK
‡ Raman Research Institute, Bangalore 560 080, India

Received 7 July 1998

Abstract. Transparent overhead-projector foil is an anisotropic material with three different principal refractive indices. Its properties can be demonstrated very simply by sandwiching the foil between crossed polarizers and looking through it at any diffusely lit surface (e.g., the sky). Coloured interference fringes are seen, organized by a pattern of rings centred on two 'bullseyes' in the directions of the two optic axes. The fringes are difference contours of the two refractive indices corresponding to propagation in each direction, and the bullseyes are degeneracies where the refractive-index surfaces intersect conically. Each bullseye is crossed by a black 'fermion brush' reflecting the sign change (geometric phase) of each polarization in a circuit of the optic axis. Simple observations lead to the determination of the three refractive indices, up to an ordering ambiguity.

1. Introduction

Hamilton's discovery of conical refraction in 1830 (Born and Wolf 1959) was a milestone in the development of the classical picture of light as a transverse wave. The phenomenon was an unexpected consequence of Fresnel's theoretical analysis of the propagation of polarized light in transparent anisotropic materials (in those days, the only such materials were crystals). According to Fresnel's theory, in any given direction two waves can propagate through the material without change. The waves have different refractive indices and orthogonal linear polarizations (we will not consider chirality here). However, there are four special directions, specified by two optic axes (along which light can propagate either way), where the two refractive indices are the same and the polarizations arbitrary, so that the material behaves as if it is isotropic. Such general materials are called biaxial; in the special case where there is one symmetry direction, the two axes coincide, and the material is uniaxial. If the refractive indices are represented as two sheets in a polar plot (the wave surface), the optic axes are singular directions where the sheets are connected. Locally the connection is like that of a double cone (a diabolo). Hamilton pointed out that this singularity gives rise to several physical phenomena, which were soon observed and studied in detail, and later incorporated into the electromagnetic description of light.

Although well understood for more than a century (Pockels 1906, Hartshorne and Stuart 1960, Bloss 1961), the phenomena are not widely known to physicists, and are regarded as obscure. This is a pity, because the connections of the cones are singularities of polarization

0143-0807/99/010001+14$19.50

optics, and so are, in a sense, at the heart of the subject. One reason for the lack of emphasis on the conical effects might be that they are rarely seen; this in turn could be because their observation was thought to require plates of biaxial crystal. One of our purposes here is to describe an extremely simple demonstration (section 2), based on an observation made by one of us (RB), by means of which some of the physics of optic axes and the associated cones can be demonstrated and explored easily.

Notwithstanding the venerable physics, there are several reasons why such a demonstration is timely, and the explanation of these is our other purpose. First, with light regarded as a stream of photons, polarization phenomena provide fine illustrations of the fundamental ideas of quantum state preparation, orthogonality, measurement, completeness and evolution; even at the classical level, it is helpful to employ a notation (section 4) reminiscent of quantum mechanics. Second, conical intersections are now being understood as organizing a wide range of quantum phenomena in solid-state physics (Simon 1983) and chemistry (Herzberg and Longuet-Higgins 1963, Teller 1937, Mead and Truhlar 1979), and it is good to recall the optical context in which they first appeared. Third, the demonstration gives immediate reality to some mathematical phenomena associated with matrices depending on parameters: degeneracies of eigenvalues, singularities in the pattern of eigenfunctions, and eigenfunction anholonomy (geometric phases). In our explanations, we will emphasize these phenomena, and give only the outline of the standard optical theory (Born and Wolf 1959, Landau *et al* 1984) of biaxial materials.

2. Experiment

The apparatus is a 'sandwich' (figure 1). Its 'bread' is two squares of polaroid sheet with their transmission directions perpendicular. Its 'filling' is a square of overhead-projector plastic transparency foil. For individual viewing, the squares can be 3 cm $\times$ 3 cm. For lecture demonstrations, the squares should be about 30 cm $\times$ 30 cm, and the whole sandwich kept flat and rigid by a 'wrapping' of clear acrylic or glass panes.

Without the filling, the sandwich is simply a pair of crossed polaroids, and transmits no light. But the inserted plastic foil is optically anisotropic—and biaxial because it has been stretched two ways during manufacture (Keller 1998). Therefore the filled sandwich is not black. The experiment consists in viewing it by transmitted diffuse light over a range of directions. An individual viewer can do this by holding the sandwich close to one eye and looking through it at a light-coloured wall, or the sky (figure 2(*a*)).

Brilliantly coloured patterns are seen. They are called conoscopic figures (Hartshorne and Stuart 1960). Looking off to the side, it becomes clear that the colours are interference

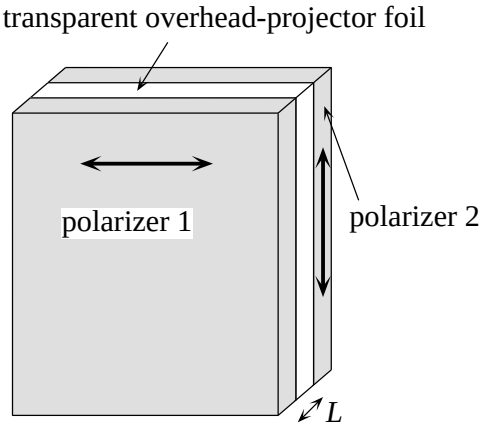

Figure 1. Structure of the black plastic sandwich.

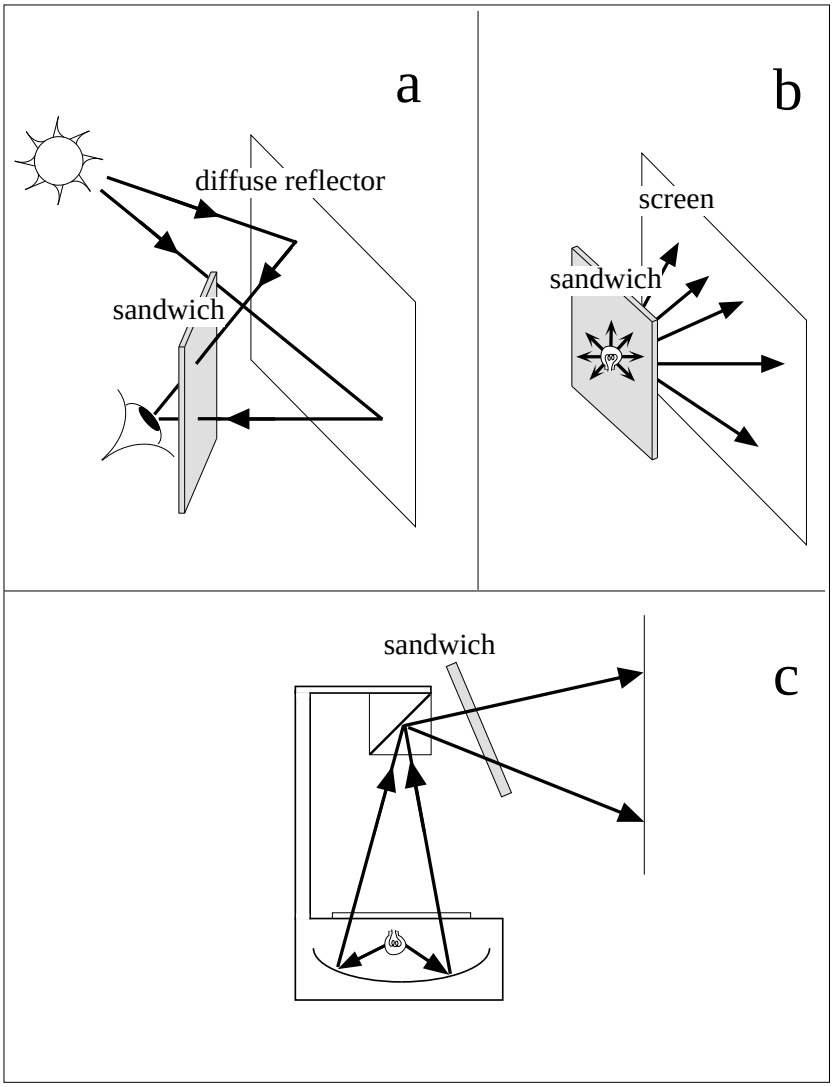

Figure 2. Observing the interference fringes. (*a*) Looking directly through the sandwich (the diffuse reflector can be the sky); (*b*) by projection from a small bright source; (*c*) to an audience, using an overhead projector.

fringes, organized about two sets of circles ('bullseyes') symmetrically disposed about the normal to the foil, separated by several tens of degrees (the precise angle depends on the type of foil). The bullseyes can be moved to the forward direction, where they can be seen more easily, by tilting the sandwich so that its normal points away from the forward direction (figure 2(*a*)). The complete pattern can be viewed by holding a small bright source of light close to the sandwich, and projecting the image onto white paper on the other side (figure 2(*b*)); the bulb from a Mini Maglite™ torch, with its lens removed, is an ideal source. (Alternatively, the complete pattern can be seen in the traditional way, with a polarizing microscope.) The individual bullseyes can be demonstrated to a large audience using the (slightly) divergent light of an overhead projector, by placing the (large) sandwich obliquely in the beam (figure 2(*c*)).

The patterns can be recorded in several ways. For their global structure, it is convenient

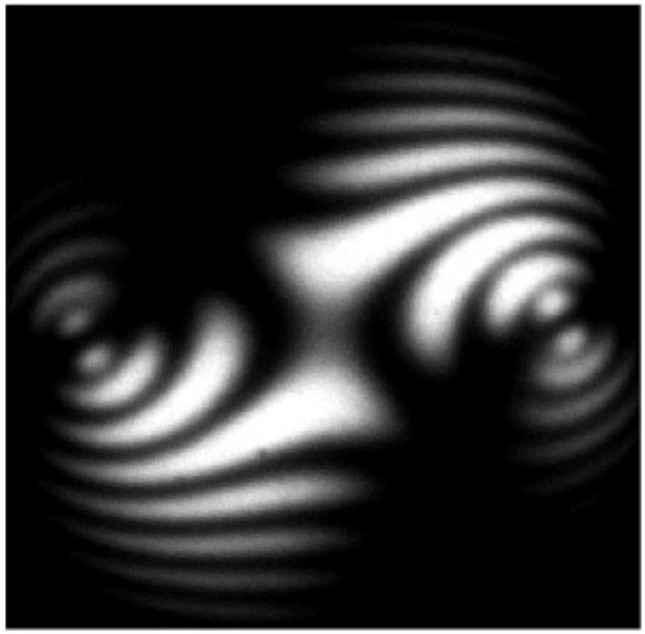

(*a*)

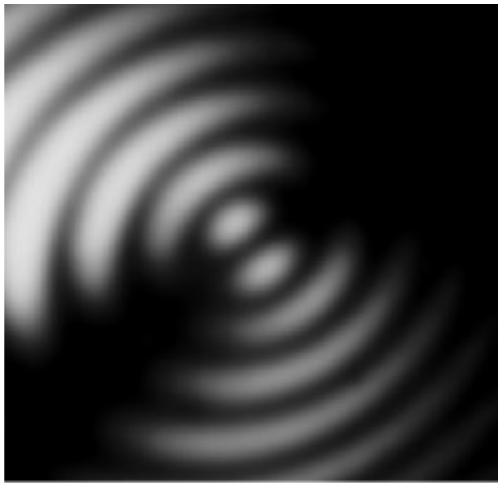

(*b*)

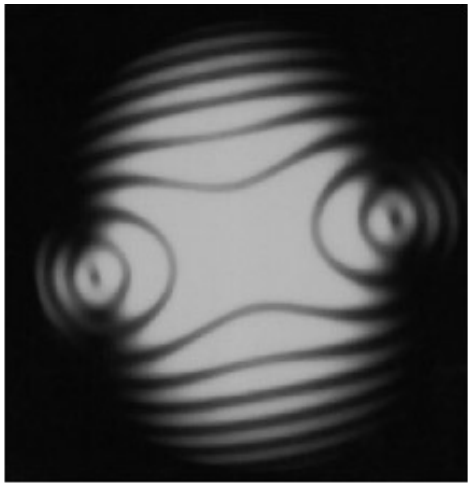

(*c*)

Figure 3. Conoscopic interference figures in monochromatic light. (*a*) Global structure, with the fringes centred on two 'bullseyes' crossed by black 'fermion brushes'; (*b*) a single bullseye; (*c*) disconnection of brushes near bullseyes for polarizer orientation near 45°.

(A colour image of a single bullseye is included in the electronic version of this article as an additional figure 9 after the list of references on page 14; see `http://www.iop.org`)

to use an arrangement like that of figure 2(*b*), with the screen replaced by a camera attached to a microscope with a wide-aperture objective lens; the details of the pattern—for example, the individual bullseyes—can be seen by magnification. Alternatively, the individual bullseyes can be photographed simply by replacing the eye in figure 2(*a*) by a camera aimed at the sky. Figure 3(*a*) shows the pattern produced by monochromatic light, and figure 3(*b*) shows

a magnification of one of the bullseyes. The main features, in addition to the interference fringes, are broad black stripes passing through the bullseyes. For a reason to be explained later, we call these the *fermion brushes*. The inclination of the brushes, relative to the line joining the bullseyes, can be altered by rotating the foil relative to the crossed polaroids.

For some foils, and certain ranges of orientation of the polarizers, the fermion brushes close to the bullseyes were disconnected (figure 3(*c*)). Superficially this resembles the effects of optical activity (Gibbs 1882, Goldhammer 1892, Pocklington 1901), in addition to the birefringence, which would break the degeneracy of the refractive indices at the optic axes. However, the details seem incompatible with this hypothesis, both in the sensitivity to polarizer orientation and the fact that the centre of the bullseye is always dark. J F Nye has suggested that the disconnection might be caused by variation of the orientation of the optic axes along the propagation path through the foil. This puzzling phenomenon (which we have not seen described in the literature) would repay investigation; we do not consider it further here.

With plastic foils we did not succeed in seeing the original phenomenon of conical refraction, namely the transformation of a narrow initial beam into a hollow cone (Born and Wolf 1959). This is because the foil is too thin: a simple calculation shows that the broadening is much less than the width of the laser beam we used, and attempts to use a stack of many foils failed because of the gaps between them and the difficulty of aligning the optic axes of successive foils.

3. Geometry and notation

Let the normal to the sandwich-filling foil define the z direction, and consider light travelling within the foil in a direction specified by the unit vector $\boldsymbol{s} = \{s_x, s_y, s_z\}$ (parallel to the wavevector), with polar angles θ, ϕ . The direction outside is obtained from $\boldsymbol{s}$ by a simple refraction correction, to be given later. It will be convenient also to denote directions by points on the plane $\boldsymbol{R} = \{X, Y\}$, with polar coordinates R, ϕ, obtained from $\boldsymbol{s}$ by stereographic projection from the south pole of the $\boldsymbol{s}$ sphere (figure 4). The equations are

$$\boldsymbol{s} = \frac{1}{1+R^2}\left\{2X, 2Y, 1-R^2\right\} \qquad R = \tan\tfrac{1}{2}\theta. \tag{1}$$

The two waves, + and −, with frequency ω and free-space wavenumber $k = \omega/c = 2\pi/\lambda$, which travel in the $\boldsymbol{s}$ direction, will be written as functions of position $\boldsymbol{r}$ and time t in terms of their electric vectors $\boldsymbol{D}$ (transverse to $\boldsymbol{s}$, unlike the electric field vector $\boldsymbol{E}$) as follows:

$$\boldsymbol{D}_\pm(\boldsymbol{s}, \boldsymbol{r}, t) = \boldsymbol{d}_\pm(\boldsymbol{s}) \exp\{\mathrm{i}kn_\pm(\boldsymbol{s})\boldsymbol{s}\cdot\boldsymbol{r} - \omega t\} \tag{2}$$

where $n_\pm(\boldsymbol{s})$ and $\boldsymbol{d}_\pm(\boldsymbol{s})$ are, respectively, the refractive indices and (orthogonal) polarizations of the waves. When we use the stereographic representation of directions, the same symbols

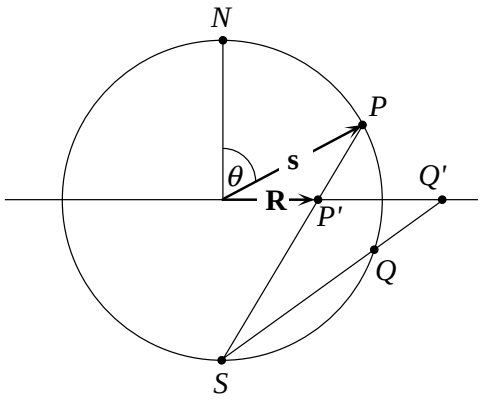

Figure 4. Stereographic projection of the wave direction from the sphere of unit vectors $\boldsymbol{s}$ to the plane $\boldsymbol{R}$, illustrated for two points P and Q (images P' and Q').

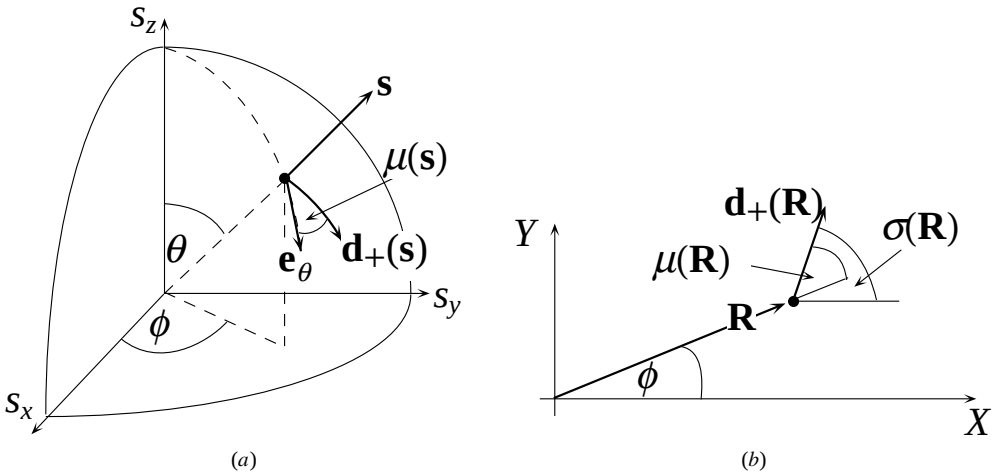

Figure 5. Directions of eigenpolarization $\boldsymbol{d}_+$. (*a*) On the $\boldsymbol{s}$ sphere, making an angle $\mu(\boldsymbol{s})$ with the unit vector $\boldsymbol{e}_\theta$. (*b*) In the $\boldsymbol{R}$ plane, making an angle $\sigma(\boldsymbol{R})$ with the X axis.

will be used, that is $n_\pm(\boldsymbol{R})$ and $\boldsymbol{d}_\pm(\boldsymbol{R})$, with the understanding that $\boldsymbol{d}_\pm(\boldsymbol{R})$ means the stereographically projected (and still orthogonal) polarizations. Where no confusion arises, we will drop the labels + and −. The polarization vector $\boldsymbol{d}_+(\boldsymbol{s})$ makes an angle $\mu(\boldsymbol{s})$ with the unit vector $\boldsymbol{e}_\theta$ on the $\boldsymbol{s}$ sphere (figure 5(*a*)), and its projection onto $\boldsymbol{R}$ makes an angle $\sigma(\boldsymbol{R}) = \mu(\boldsymbol{R}) + \phi$ with the X axis (figure 5(*b*)), where $\mu(\boldsymbol{R}) = \mu(\boldsymbol{s})$ (because the projection preserves angles) (for $\boldsymbol{d}_-$, $\pi/2$ must be added to these angles). Thus

$$\boldsymbol{d}_+(\boldsymbol{s}) = \boldsymbol{e}_\theta \cos\mu + \boldsymbol{e}_\phi \sin\mu \qquad \boldsymbol{d}_+(\boldsymbol{R}) = \boldsymbol{e}_X \cos\sigma + \boldsymbol{e}_Y \sin\sigma. \tag{3}$$

Since $\boldsymbol{d}$ and $-\boldsymbol{d}$ represent the same polarization, all physical quantities derived from $\boldsymbol{d}$ must be invariant under changes of μ and ϕ by π.

The foil is an anisotropic transparent dielectric of thickness L, specified by its constitutive relation, which we write in the form

$$\boldsymbol{D} = \varepsilon_0 \mathbf{n}^2 \boldsymbol{E} \tag{4}$$

where $\mathbf{n}^2$ is the dimensionless dielectric tensor, written in terms of the three principal refractive indices as

$$\mathbf{n}^2 = \begin{pmatrix} n_x^2 & 0 & 0 \\ 0 & n_y^2 & 0 \\ 0 & 0 & n_z^2 \end{pmatrix}. \tag{5}$$

We choose the y axis such that n_y is the intermediate-valued principal index; this will make the bullseyes lie on the X axis. Moreover, we make the asumption $n_x < n_z$, and will discuss this at the end of section 6. Thus

$$n_x < n_y < n_z. \tag{6}$$

It will be convenient to define

$$\alpha \equiv \frac{1}{n_x^2} - \frac{1}{n_y^2} \qquad \beta \equiv \frac{1}{n_y^2} - \frac{1}{n_z^2}. \tag{7}$$

Although we shall work with exact formulae, we note that in the foil $\alpha \ll 1$ and $\beta \ll 1$.

Finally, the polarizers will be specified by their orientations γ and $\gamma + \pi/2$ with respect to the X axis.

4. Theory: intensity variation

The observed pattern is the intensity $I(\boldsymbol{R}, \gamma)$ of the light when it emerges from the sandwich after travelling in the direction R, with the orientation of the polarizers specified by γ. When calculating $I(\boldsymbol{R}, \gamma)$, it is convenient to use vectors $\boldsymbol{V}$ to represent the $\boldsymbol{D}$ vector of the light as it traverses the foil; we think of $\boldsymbol{V}$ as the column vector representing $\boldsymbol{D}$, and denote by $\boldsymbol{V}^{\mathrm{T}}$ the corresponding row vector (transpose). $\boldsymbol{V}$ and $\boldsymbol{V}^{\mathrm{T}}$ are analogous to the ket and bra in quantum mechanics; thus the dot product $\boldsymbol{U} \cdot \boldsymbol{V}$ can alternatively be written $\boldsymbol{U}^{\mathrm{T}}\boldsymbol{V}$.

The first polarizer projects $\boldsymbol{V}$ onto a state of linear polarization, represented by a vector $\boldsymbol{P}$. In quantum mechanics, this step is the preparation of the state. As the light enters the anisotropic foil, we resolve its state $\boldsymbol{P}$ into components along the two eigenpolarizations $\boldsymbol{d}_{\pm}(\boldsymbol{R})$. These are complete and orthonormal, i.e.

$$\begin{aligned} &\boldsymbol{d}_{+}(\boldsymbol{R})\boldsymbol{d}_{+}^{\mathrm{T}}(\boldsymbol{R}) + \boldsymbol{d}_{-}(\boldsymbol{R})\boldsymbol{d}_{-}^{\mathrm{T}}(\boldsymbol{R}) = \mathsf{I} \\ &\boldsymbol{d}_{\pm}(\boldsymbol{R}) \cdot \boldsymbol{d}_{\pm}(\boldsymbol{R}) = 1 \qquad \boldsymbol{d}_{\pm}(\boldsymbol{R}) \cdot \boldsymbol{d}_{\mp}(\boldsymbol{R}) = 0. \end{aligned} \tag{8}$$

The resolution is

$$\boldsymbol{P} = \left(\boldsymbol{d}_{+}(\boldsymbol{R})\boldsymbol{d}_{+}^{\mathrm{T}}(\boldsymbol{R}) + \boldsymbol{d}_{-}(\boldsymbol{R})\boldsymbol{d}_{-}^{\mathrm{T}}(\boldsymbol{R})\right)\boldsymbol{P} = \boldsymbol{d}_{+}(\boldsymbol{R}) \cdot \boldsymbol{P}\, \boldsymbol{d}_{+}(\boldsymbol{R}) + \boldsymbol{d}_{-}(\boldsymbol{R}) \cdot \boldsymbol{P}\, \boldsymbol{d}_{-}(\boldsymbol{R}). \tag{9}$$

The polarizations + and − propagate independently through the foil, and acquire phases determined by their refractive indices $n_{\pm}(\boldsymbol{R})$. The graphs of these two functions, either as polar plots (that is, as radial distances for direction $\boldsymbol{s}$), or perpendicular to the $\boldsymbol{R}$ plane, are the sheets of the refractive-index (wave) surface. Since the distance travelled in the foil is

$$L(\boldsymbol{s}) = \frac{L}{\cos\theta} \equiv L(\boldsymbol{R}) = L\left(\frac{1 + R^2}{1 - R^2}\right) \tag{10}$$

the polarizations become

$$\boldsymbol{d}_{\pm}(\boldsymbol{R}) \to \boldsymbol{d}_{\pm}(\boldsymbol{R}) \exp\{\mathrm{i}kn_{\pm}(\boldsymbol{R})L(\boldsymbol{R})\} \equiv \boldsymbol{d}_{\pm}(\boldsymbol{R}) \exp\{\mathrm{i}\chi_{\pm}(\boldsymbol{R})\}. \tag{11}$$

In quantum mechanics, this step is the evolution of the state, governed by the Schrödinger equations (here Maxwell's equations). Thus the state after propagation through the foil, and before entering the second polarizer, is

$$\boldsymbol{V}(\boldsymbol{R}) = \boldsymbol{d}_{+}(\boldsymbol{R}) \cdot \boldsymbol{P}\, \boldsymbol{d}_{+}(\boldsymbol{R}) \exp\{\mathrm{i}\chi_{+}(\boldsymbol{R})\} + \boldsymbol{d}_{-}(\boldsymbol{R}) \cdot \boldsymbol{P}\, \boldsymbol{d}_{-}(\boldsymbol{R}) \exp\{\mathrm{i}\chi_{-}(\boldsymbol{R})\}. \tag{12}$$

The second polarizer projects $\boldsymbol{V}$ onto a state represented by a vector $\overline{\boldsymbol{P}}$, perpendicular to the first polarizer $\boldsymbol{P}$, i.e.

$$\overline{\boldsymbol{P}} \cdot \boldsymbol{P} = 0. \tag{13}$$

In quantum mechanics, this step is the measurement of the state. The desired intensity is

$$I(\boldsymbol{R}, \gamma) = \left|\overline{\boldsymbol{P}} \cdot \boldsymbol{V}(\boldsymbol{R})\right|^2 \tag{14}$$

and a short calculation using (8) and (13) leads to

$$I(\boldsymbol{R}, \gamma) = 4\left[\boldsymbol{d}_{+}(\boldsymbol{R}) \cdot \overline{\boldsymbol{P}}\right]^2\left[\boldsymbol{d}_{+}(\boldsymbol{R}) \cdot \boldsymbol{P}\right]^2 \sin^2\left\{\tfrac{1}{2}\Delta\chi(\boldsymbol{R})\right\} \tag{15}$$

where

$$\Delta\chi(\boldsymbol{R}) \equiv \chi_{+}(\boldsymbol{R}) - \chi_{-}(\boldsymbol{R}) = kL(\boldsymbol{R})\left[n_{+}(\boldsymbol{R}) - n_{-}(\boldsymbol{R})\right]. \tag{16}$$

To calculate this intensity explicitly, it is convenient to imagine the foil as fixed, and the orientation of the polarizers as variable. Let the first polarizer have orientation γ: this means that it transmits light whose electric $\boldsymbol{D}$ vector is oriented at an angle γ to the X axis in the $\boldsymbol{R}$ plane. The second polarizer transmits light in the perpendicular direction, i.e. $\gamma + \pi/2$. Thus in equation (15)

$$P = (\cos\gamma,\ \sin\gamma) \qquad \overline{\boldsymbol{P}} = (\sin\gamma,\ -\cos\gamma). \tag{17}$$

With the polarization $\boldsymbol{d}_+(\boldsymbol{R})$ as defined in (3), equation (15) gives

$$I(\boldsymbol{R},\gamma) = \sin^2\left\{2\big(\gamma - \sigma(\boldsymbol{R})\big)\right\}\sin^2\left\{\tfrac{1}{2}\Delta\chi(\boldsymbol{R})\right\}. \tag{18}$$

In equation (18), the second factor describes the fringes resulting from the interference of the two polarizations that emerge from the foil, when projected onto the common state $\overline{\boldsymbol{P}}$. From equation (16), these fringes are approximately contours of difference of the two refractive indices (the $\boldsymbol{R}$ dependence of L gives only a small correction). The thicker the foil, or the shorter the wavelength λ, the closer the fringes. Because of the λ dependence, the fringes are coloured (the λ dependence of the refractive indices, i.e. dispersion of the optic axes, is a much smaller effect). Close to the conical singularities of the two refractive-index sheets where $n_+ = n_-$, the contours are closed loops (actually circles); these are the bullseyes that reveal the singularities and dominate the images.

The first factor in (18) vanishes along the lines where $\sigma(\boldsymbol{R}) = \gamma \pmod{\pi/2}$. These are the black brushes, called isogyres, which therefore reveal the polarization directions at $\boldsymbol{R}$: as the crossed polarizers are rotated relative to the foil, the brushes sweep through all these directions. We shall see that in a circuit of the singularity (in $\boldsymbol{R}$ space) σ changes by π; this implies that for each γ the brush crosses the bullseye in a single smooth line. Note that equation (18) is unaltered if γ or σ is changed by $\pi/2$, reflecting invariance of the physics under exchange of the two polarizers $\boldsymbol{P}$ and $\overline{\boldsymbol{P}}$ or the two polarizations $\boldsymbol{d}_+$ and $\boldsymbol{d}_-$.

5. Theory: fringes, isogyres and the fermion brush

With the electric vector $\boldsymbol{D}$ (2), and the constitutive equation (4), Maxwell's equations reduce to

$$\boldsymbol{d}(\boldsymbol{s}) + n^2(\boldsymbol{s})\boldsymbol{s}\times\boldsymbol{s}\times\boldsymbol{\eta}^{-2}\boldsymbol{d}(\boldsymbol{s}) = 0 \tag{19}$$

where $\boldsymbol{d}$ denotes $\boldsymbol{d}_+$ or $\boldsymbol{d}_-$. Although this represents three linear equations, transversality implies that the consistency condition (vanishing determinant of the operator in (19)) leads to two, not three refractive indices $n(\boldsymbol{s})$ for each $\boldsymbol{s}$ (the third would be infinite, corresponding to electrostatic fields rather than waves). These two indices $n_\pm(\boldsymbol{s})$ are given by the eigenvalues of the part of the matrix $\boldsymbol{\eta}^{-2}$ transverse to $\boldsymbol{s}$; the corresponding eigenvectors are the polarizations $\boldsymbol{d}_\pm(\boldsymbol{s})$.

A long calculation, using the first equation in (3) to represent $\boldsymbol{d}$, and the definitions (5) and (7), leads to a formula in which the refractive index surfaces are conveniently expressed in terms of the positions of the four optic axes. In the $\boldsymbol{R}$ plane, these are at

$$Y = 0 \qquad X = \pm X_{\rm c},\ \pm\frac{1}{X_{\rm c}} \qquad X_{\rm c} \equiv \sqrt{1+\frac{\beta}{\alpha}} - \sqrt{\frac{\beta}{\alpha}}. \tag{20}$$

On the $\boldsymbol{s}$ sphere, the axes are

$$\phi = 0,\ \pi \qquad \theta = \theta_{\rm c},\ \pi - \theta_{\rm c} \qquad \tan\theta_{\rm c} = \sqrt{\frac{\alpha}{\beta}}. \tag{21}$$

The indices are

$$\begin{aligned}
&\frac{1}{n_\pm^2(\boldsymbol{s})} = \frac{1}{n_y^2} - \frac{\alpha}{2(1+R^2)^2}\left\{H \pm \sqrt{G}\right\}\\
&H \equiv (X^2 - X_{\rm c}^2)\left(X^2 - \frac{1}{X_{\rm c}^2}\right) - 4Y^2\frac{\beta}{a}\\
&G \equiv 64X^2Y^2\frac{\beta}{a}\left(1+\frac{\beta}{a}\right) + \left[H + Y^2\left(2(1+X^2) + 8\frac{\beta}{\alpha} + Y^2\right)\right]^2.
\end{aligned} \tag{22}$$

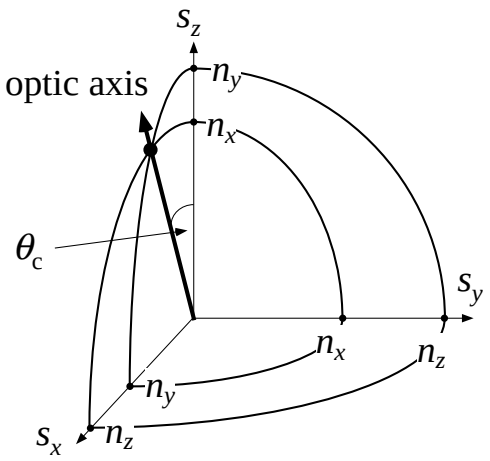

Figure 6. Refractive index surfaces in direction space, showing the optic axis (degeneracy) where the surfaces intersect conically.

This formula incorporates the following special cases, illustrated in figure 6 for an octant of the $\boldsymbol{s}$ sphere:

$$\begin{aligned} &X = X_c,\ Y = 0 \ \text{(waves along optic axes):} && n_+ = n_- = n_y \\ &X = Y = 0 \ \text{(waves along } \boldsymbol{e}_z\text{):} && n_+ = n_y,\ n_- = n_x \\ &X = 1,\ Y = 0 \ \text{(waves along } \boldsymbol{e}_x\text{):} && n_+ = n_z,\ n_- = n_y \\ &X = 0,\ Y = 1 \ \text{(waves along } \boldsymbol{e}_y\text{):} && n_+ = n_z,\ n_- = n_x. \end{aligned} \tag{23}$$

Close to the optic axes, equation (22) can be simplified to display the form of the conical intersections explicitly. We find

$$\begin{aligned} n_\pm(\boldsymbol{R}) &\approx n_y \left[1 + C\left\{\pm\sqrt{(X - X_c)^2 + Y^2} - (X - X_c)\right\}\right] \\ C &\equiv \frac{\sqrt{(n_y^2 - n_x^2)(n_z^2 - n_y^2)}}{\sqrt{(n_z^2 - n_x^2)}\left[\sqrt{(n_z^2 - n_x^2)} - \sqrt{(n_z^2 - n_y^2)}\right]}. \end{aligned} \tag{24}$$

The fact that the coefficients of $(X - X_c)^2$ and Y^2 in the square root are the same shows that the cones are circular near their intersection (in both the $\boldsymbol{R}$ and $\boldsymbol{s}$ spaces).

The polarizations (isogyres) $\boldsymbol{d}$ are the eigenvectors defined by (19). Geometrically, these are the principal axes of the ellipse defined by the intersection of the plane normal to s with the indicatrix (Nye 1995). On the $\boldsymbol{s}$ sphere (figure 5(*a*)) these are specified by the angle $\mu(\boldsymbol{s})$. A calculation from (19) gives

$$\tan 2\mu(\boldsymbol{s}) = \frac{\sin 2\phi \cos\theta}{(\beta/\alpha)\sin^2\theta - \cos 2\phi \cos^2\theta}. \tag{25}$$

This gives both polarizations (with μ values differing by 2π). At the optic axes (21), the numerator and denominator vanish, so that the pattern of isogyres is singular.

In the projective plane, where $\boldsymbol{d}$ is specified by the angle $\sigma(\boldsymbol{R})$, equation (25) can be cast in an interesting form by introducing the complex direction variable

$$\zeta \equiv X + \mathrm{i}Y \tag{26}$$

and the following complex function with zeros at each of the optic axes:

$$A(\zeta) \equiv (1 - \zeta^2)^2 - 4\zeta^2\,\frac{\beta}{\alpha} = (\zeta^2 - X_c^2)\left(\zeta^2 - \frac{1}{X_c^2}\right). \tag{27}$$

Then the isogyres (now denoted $\sigma(\zeta)$) satisfy

$$\mathrm{Im}\, A(\zeta) \exp\{-2\mathrm{i}\sigma(\zeta)\} = 0. \tag{28}$$

From this we can find a function $B(\zeta)$ whose real and imaginary parts have the isogyres as their contours. For if we choose $\exp -\mathrm{i}\sigma = B'(\zeta) = 1/\sqrt{A}$, then $\nabla \mathrm{Re}\, B = \{\cos\sigma, \sin\sigma\}$ and $\nabla \mathrm{Im}\, B = \{-\sin\sigma, \cos\sigma\}$. The function is

$$B(\zeta) = \int_0^\zeta \frac{\mathrm{d}\zeta}{\sqrt{A(\zeta)}} = X_\mathrm{c} F\left(\arcsin\frac{\zeta}{X_\mathrm{c}},\ X_\mathrm{c}^4\right) \tag{29}$$

where F denotes the elliptic integral (we use the convention in *Mathematica*™ (Wolfram 1991)).

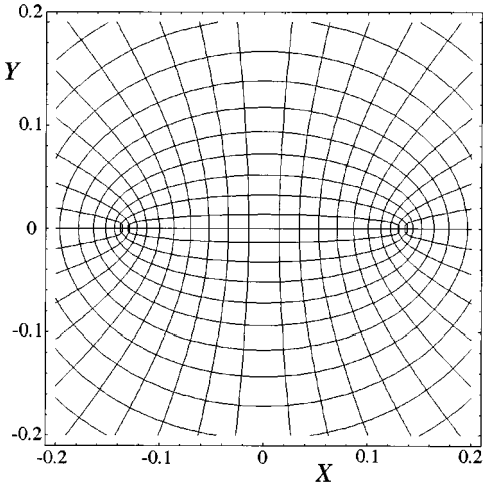

Figure 7. Isogyres in the projective plane, calculated for $n_x = 1.563$, $n_y = 1.58$, $n_z = 1.883$; the optic axes are at $X_\mathrm{c} = 0.133$, corresponding to an angle $\theta_\mathrm{c} = 13.4^\circ$.

Figure 7 shows the orthogonal net of polarization directions, computed from (29), for a range that includes the two optic axes in the northern hemisphere of the $\boldsymbol{s}$ plane. The pattern is dominated by the singularities at $\pm X_\mathrm{c}$. Around a circuit of each singularity, each of the two polarizations rotates by π in the same sense as the circuit. This means that each singularity has index $+1/2$; it cannot be otherwise, because the total index of singularities of a line field on a sphere must, by the 'hairy sphere' theorem (Spivak 1975, Iyanaga and Kawada 1968), be +2 (the Euler–Poincaré characteristic of a sphere), and so each of the four identical optic-axis singularities must have index $+1/2$. In one classification of the singularities of line fields (Berry and Hannay 1977, Berry and Upstill 1980), these are 'lemons'; the terminology arose in connection with umbilic points on surfaces (Darboux 1896, see also the historical remarks in Berry 1989).

In the image intensity (18), the first factor can be written explicitly by means of (28) as

$$\sin^2\{2(\gamma - \sigma(\boldsymbol{R}))\} = \frac{1}{2}\left\{1 + \frac{\left[\mathrm{Im}^2 A(\zeta) - \mathrm{Re}^2 A(\zeta)\right]\cos 4\gamma - 2\mathrm{Re}\, A(\zeta)\mathrm{Im}\, A(\zeta)\sin 4\gamma}{\left|A(\zeta)\right|^2}\right\}. \tag{30}$$

Now the full intensity can be calculated from (18), (16), (10) and (22), and rendered as density plots to simulate the observations (e.g., those in figure 3). Three such simulations, for different values of the polarizer orientation γ, are shown in figure 8(*a–c*); they should be compared with the experimental figure 3(*a*), whose conditions they have been chosen to match, as will be explained in section 6.

The most striking features are the two bullseyes, centred on the optic axes. Figure 8(*d*) shows a magnification of one of these. We have already mentioned the broad black brush

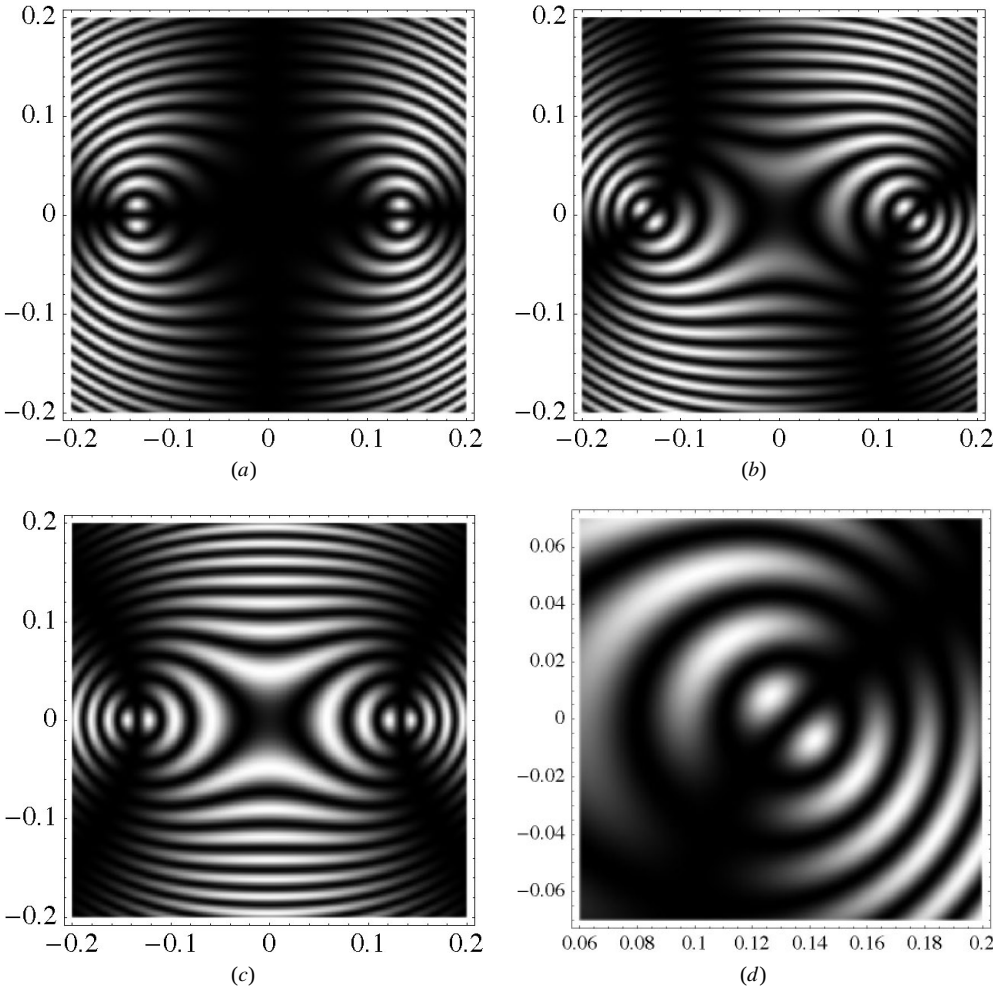

Figure 8. Simulations of the conoscopic figures, calculated from equation (18) as density plots of the intensity $I(\boldsymbol{R}, \gamma)$ for the same conditions as in figure 7, with $\lambda = 0.546\ \mu$m, $L = 100\ \mu$m. (*a*) $\gamma = 0$; (*b*) $\gamma = \pi/8$; (*c*) $\gamma = \pi/4$. A magnification of one of the bullseyes in (*b*) is shown in (*d*).

through the centre. This has its origin in the first factor in (18). During a circuit of the bullseye, the black brush will be encountered whenever $\sigma(R) = \gamma$ (modulo $\pi/2$). Because the singularity of the pattern of polarizations has index $1/2$, $\sigma(\boldsymbol{R})$ changes by π around such a circuit, so the brush condition will be satisfied twice. Now, close to the bullseye the change in $\sigma(\boldsymbol{R})$ is uniform for a circular circuit; this follows from the square root singularity in (29) with (27). Therefore these two encounters will be on opposite sides of the bullseye, resulting in in a single black line passing through it smoothly. In local polar coordinates R_{local}, ϕ_{local}, the intensity of light emerging near the bullseye is

$$I(\boldsymbol{R}, \gamma) \approx \sin^2(2\gamma - \phi_{\mathrm{local}}) \sin^2(D R_{\mathrm{local}}) \qquad (\boldsymbol{R} \approx \{X_{\mathrm{c}},\ 0\}) \tag{31}$$

where in the second factor D is a constant and the circularity of the cones (equation (24)) has been invoked.

So, the black brushes are consequences of the fact that the eigenvectors $\boldsymbol{d}$ of Maxwell's equation (19) are not single-valued, but reverse round a circuit of each bullseye. The reversal

corresponds to a sign change in each eigenvector, i.e. a phase change of π. Such sign changes are universally present (Arnold 1978, Uhlenbeck 1976) during a circuit of a simple degeneracy of a real symmetric matrix (the operator in (19) can be expressed this way by a simple transformation), with two eigenvalues that coincide linearly. They are the simplest example of a geometric phase (Pancharatnam 1956, Berry 1984, Shapere and Wilczek 1989), and mathematically identical to the sign change on rotation of quantum particles with half-integer spin (Silverman 1980); that is why we call the black lines fermion brushes. In optics this fact that the polarization states have 4π spinor symmetry, even though photons are spin-1 particles, has been demonstrated experimentally (Bhandari 1993a, 1997).

We emphasize that the fermion brushes occur here because the foil we use is biaxially anisotropic. If the material were uniaxial, as in plastic threads made by stretching in one direction, rather than two, this would correspond to confluence of the two optic axes, where the singularities would each have strength +1 instead of +1/2 (the total index on the $\boldsymbol{s}$ sphere would still be +2). Then the eigenvectors s would be single-valued, and the brush condition from (18) would be satisfied four times, rather than twice, in a circuit of each axis. Therefore each bullseye would be traversed by a black cross rather than a single black line, as is well known for uniaxial materials (Born and Wolf 1959) (in (31) this situation can be described locally by replacing ϕ_{local} by $2\phi_{\text{local}}$).

Bullseyes are not the only singularities of polarization optics. Consider propagation through the foil as described by a 2×2 unitary (Jones) matrix $\mathbf{U}$, depending on $\boldsymbol{R}$, whose eigenangles are $\pm\frac{1}{2}\Delta\chi(\boldsymbol{R})$ (equation (16)). Degeneracies of $\mathbf{U}$ are the dark rings of the conoscopic figures, where $\frac{1}{2}\Delta\chi$ is a multiple of π; if the multiple is even $\mathbf{U}$ has eigenvalues +1, and if it is odd $\mathbf{U}$ has eigenvalues -1 (Bhandari and Love 1994). Special among these are the bullseyes: points in $\boldsymbol{R}$ where $\Delta\chi = 0$ (eigenvalues +1) because of the equality (degeneracy) of the two refractive indices $n_\pm$. A different sort of singularity, observed in interference experiments (Bhandari 1992a, b, 1993b) and yielding a phase change of 2π rather than π, occurs when two interfering polarization states become orthogonal, so that according to Pancharatnam's definition (Pancharatnam 1956) a relative phase cannot be defined. In the present context these singularities are the rows of bright points of conoscopic figures between crossed polarizers (where the 'anti-isogyres' cross the bright rings) or the points of zero intensity between parallel polarizers.

6. Characterizing the foil

We seek the three refractive indices $n_x,\ n_y,\ n_z$. Many precise methods are available for this, described in detail in standard texts (Pockels 1906, Hartshorne and Stuart 1960, Bloss 1961). Our aim here is to show how a rough estimate of n_x, n_y and n_z can be obtained with simple naked-eye observations. The three indices differ by small amounts, i.e. in equation (7) $\alpha \ll 1$ and $\beta \ll 1$. Therefore the average index, which determines optical effects not involving polarization, can be chosen as n_y. We measured this by the longitudinal shift of an image viewed through a stack of foils, with the films wetted with oil to reduce reflections from the interfaces; the result was $n_y = 1.57 \pm 0.01$, identical to the tabulated value for polycarbonate (Kroschwitz 1987).

The remaining two refractive indices can be determined as follows. First, by measuring the angle $2\theta_{\text{external}}$ between the bullseyes, the ratio α/β can be obtained from (21), using Snell's law for the refraction correction relating θ_{external} to the direction θ_{c} of the optic axes in the foil:

$$\sin\theta_{\text{external}} = n_y \sin\theta_{\text{c}}. \tag{32}$$

For the foil that generated the bullseyes in figure 3(*a*), we measured $\theta_{\text{external}} = (24 \pm 1)^\circ$, giving $\alpha/\beta = 0.07$. Second, the phase difference between the two waves travelling normal to the foil can be determined from the number N of fringes between the bullseye ($X = X_{\text{c}}$) and the centre of the pattern (at $X = 0$) where the two waves have zero phase difference. N need not be an integer, and is easiest to estimate by counting dark fringes. From equations (15) and

(16), this gives

$$n_y - n_x = \frac{N\lambda}{L}. \tag{33}$$

From figure 3(*a*), $N \approx 3.1$, and since the foil has thickness 0.1 mm we find, for $\lambda = 0.546\ \mu$m, $n_y - n_x = 0.017$.

Collecting these results, for the foil we used (Niceday Write-on OHP film) we find

$$n_x = 1.553 \qquad n_y = 1.57 \qquad n_z = 1.88. \tag{34}$$

Although two of the values are close together, the rather large angle between the optic axes indicates that the foil is far from uniaxial. The large index corresponds to waves whose $\boldsymbol{D}$ vector is normal to the foil.

At this point we encounter an annoying ambiguity, related to the ordering of the refractive indices $n_x,\ n_y,\ n_z$, and known in the literature as the problem of the optic sign (Bloss 1961). The observation of bullseyes rules out the possibility that the intermediate index corresponds to the direction normal to the foil (if it did, the optic axes would lie in the plane of the foil); this motivated our conventional choice of n_y as the intermediate index. For the remaining indices, we made the assumption $n_x < n_z$ (equation (6)), that is, the smallest refractive index corresponds to waves polarized in the plane of the foil. But what if the opposite is true, i.e. $n_x > n_z$? Then α and β would both be negative; but this would leave unaffected the ratio determining the axis θ_c according to (21). Incorporating the measurement of the fringe number N, we find that if a and b are small but otherwise arbitrary, the following two situations cannot be distinguished by the pattern of bullseyes they produce:

$$\begin{aligned} &\{(n_y - a)(= n_x),\ n_y,\ (n_y + b)(= n_z)\} \\ &\{(n_y - b)(= n_z),\ n_y,\ (n_y + a)(= n_x)\}. \end{aligned} \tag{35}$$

If a and b are different, these represent physically different materials. We think that this ambiguity could be resolved only by a much more accurate experiment than those envisaged here, equivalent to directly measuring the indices n_x and n_y by the lateral shifts of images seen through a stack of foils, using x- and y-polarized light, and seeing which is the larger. In the present case, the alternative determination gives physically unacceptable indices, namely 1.60, 1.58 and 1.28 (the lowest value—less than that of water—is too small for a plastic).

Acknowledgment

We thank Professor J F Nye for a careful reading of the manuscript.

References

Arnold V I 1978 *Mathematical Methods of Classical Mechanics* (Berlin: Springer)
Berry M V 1984 Quantal phase factors accompanying adiabatic changes *Proc. R. Soc.* A **392** 45–57.
——1989 *Geometric Phases in Physics* ed A Shapere and F Wilczek (Singapore: World Scientific) pp 7–28
Berry M V and Hannay J H 1977 Umbilic points on Gaussian random surfaces *J. Phys. A: Math. Gen.* **10** 1809–21
Berry M V and Upstill C 1980 Catastrophe optics: morphologies of caustics and their diffraction patterns *Progr. Opt.* **18** 257–346
Bhandari R 1992a Observation of Dirac singularities with light polarization. I *Phys. Lett.* A **171** 262–6
——1992b Observation of Dirac singularities with light polarization. II *Phys. Lett.* A **171** 267–70
——1993a 4p spinor symmetry—some new observations *Phys. Lett.* A **180** 15–20
——1993b Interferometry without beam splitters—a sensitive technique for spinor phases *Phys. Lett.* A **180** 21–4
——1997 Polarization of light and topological phases *Phys. Rep.* **281** 1–64
Bhandari R and Love J 1994 Polarization eigenmodes of a QHQ retarder—some new features *Opt. Commun.* **10** 479–84
Bloss F D 1961 *An Introduction to the Methods of Optical Crystallography* (New York: Holt, Rinehart and Winston)
Born M and Wolf E 1959 *Principles of Optics* (Oxford: Pergamon)
Darboux G 1896 *Lecons sur la theorie des surfaces* (Paris: Gauthier-Villars)

Gibbs J W 1882 On double refraction in perfectly transparent media which exhibit the phenomenon of circular polarization *Am. J. Sci. (ser. 3)* **23** 460–76
Goldhammer M D 1892 Theorie electromagnetique de la polarisation roratiore naturelle des corps transparents *J. Physique Theor. Appl. (ser. 3)* **1** 205–9
Hartshorne N H and Stuart A 1960 *Crystals and the Polarising Microscope* (London: Arnold)
Herzberg G and Longuet-Higgins H C 1963 Intersection of potential-energy surfaces in polyatomic molecules *Disc. Faraday Soc.* **35** 77–82
Iyanaga S and Kawada Y (ed) 1968 *Encyclopedic Dictionary of Mathematics* (Cambridge, MA: MIT Press)
Keller A 1998 Private communication
Kroschwitz J I (ed) 1987 *Encyclopedia of Polymer Science and Engineering* (New York: Wiley)
Landau L D, Lifshitz E M and Pitaevskii L P 1984 *Electrodynamics of Continuous Media* (Oxford: Pergamon)
Mead C A and Truhlar D G 1979 On the determination of Born–Oppenheimer nuclear motion wave functions including complications due to conical intersections and identical nuclei *J. Chem. Phys.* **70** 2284–96
Nye J F 1995 *Physical Properties of Crystals* (Oxford: Clarendon) ch 13 and appendix H
Pancharatnam S 1956 Generalized theory of interference, and its applications. Part I. Coherent pencils *Proc. Ind. Acad. Sci.* A **44** 247–62
Pockels F 1906 *Lehrbuch der Kristalloptik* (Leipzig: Teubner)
Pocklington H C 1901 On rotatory polarization in biaxial crystals *Lond., Edin. Dublin Phil. Mag. J. Sci. (ser. 2)* **2** 361–70
Shapere A and Wilczek F (ed) 1989 *Geometric Phases in Physics* (Singapore: World Scientific)
Silverman M 1980 The curious problem of spinor rotation *Eur. J. Phys.* **1** 116–23
Simon B 1983 Holonomy, the quantum adiabatic theorem, and Berry's phase *Phys. Rev. Lett.* **51** 2167–70
Spivak M 1975 *A Comprehensive Introduction to Differential Geometry* (San Francisco, CA: Publish or Perish)
Teller E 1937 The crossing of potential surfaces *J. Phys. Chem.* **41** 109–16
Uhlenbeck K 1976 Generic properties of eigenfunctions *Am. J. Math.* **98** 1059–78
Wolfram S 1991 *Mathematica* (Reading, MA: Addison-Wesley)

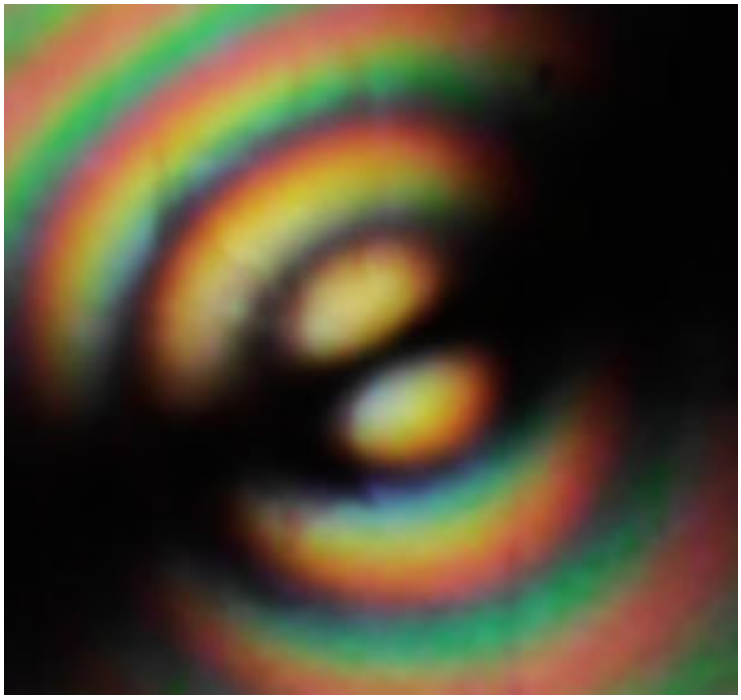

Figure 9. Colour image of conoscopic interference in white light for a single bullseye.